Heyd-Scuseria-Ernzerhof hybrid functional for calculating the lattice dynamics of semiconductors

Kerstin Hummer,* Judith Harl, and Georg Kresse
Department of Computational Materials Physics, Universität Wien, Sensengasse 8/12, A-1090 Wien, Austria
(Received 9 May 2009; revised manuscript received 12 August 2009; published 14 September 2009)

We present an *ab initio* study of the lattice dynamics of group-IV elemental semiconductors and insulators using a finite differences approach. The investigated solids include cubic diamond (C), silicon (Si), germanium (Ge), and the zero-gap semiconductor gray tin (α-Sn). The main objective of this work is to examine the performance of the screened hybrid functional (HSE) proposed by Heyd, Scuseria, and Ernzerhof [J. Chem. Phys. **118**, 8207 (2003); J. Chem. Phys. **124**, 219906(E) (2006)] for calculating phonon-dispersion relations. We find that all local and semilocal functionals tend to underestimate the phonon frequencies, with the errors increasing with increasing atomic mass. For α-Sn, semilocal functionals even qualitatively fail to describe the dispersion of the highest optical phonon mode. We show that this is related to semilocal functionals predicting α-Sn to be a metal, whereas experimentally it is a zero-gap semiconductor. The HSE functional yields the correct electronic band structure resulting in qualitatively correct phonon-dispersion relations for all four solids. Quantitatively, the phonon frequencies are slightly overestimated using HSE, in particular for the lighter elements C and Si. Our results are compared to previously reported theoretical findings.

DOI: 10.1103/PhysRevB.80.115205 PACS number(s): 63.20.dk, 71.15.Mb, 71.20.Mq, 71.20.Nr

I. INTRODUCTION

The first-principles calculation of lattice dynamical properties within electronic structure theory requires either the evaluation of second derivatives or a very precise determination of the Hellmann-Feynman forces acting on the atomic cores in the solid due to the displacement of a single atom in a large supercell (finite differences). For extended systems, this was commonly achieved within Kohn-Sham density functional theory (KS-DFT) (Refs. 1 and 2) utilizing the standard approximations for the exchange-correlation (*xc*) energy functional E_{xc}, i.e., the local density approximation (LDA) (Refs. 2–4) or the generalized gradient approximation (GGA), where the most common one is the Perdew-Burke-Ernzerhof (PBE) form.[5,6] Both rely on the *xc* energy per particle of the *uniform* electron gas with density $n(\mathbf{r})$ and thus are expected to be useful for systems with slowly varying densities only (so-called *local/semilocal* functionals). Nevertheless, they have proven to be rather *universally* applicable in theoretical materials science and achieve fairly good accuracy for ionization energies of atoms, dissociation energies of molecules, and cohesive energies, as well as bond lengths and geometries of molecules and solids.[7–9] This unexpectedly good performance of DFT-LDA/GGA for the ground-state properties of many materials is due to partial error cancellation in the *x* and *c* energy parts.

One problem of the two most commonly applied functionals—LDA and PBE—is that LDA consistently underestimates the lattice constants of solids, an effect that is commonly referred to as *overbinding*,[10] whereas PBE almost always overestimates the volume. Compared to experiment, the errors typically amount to 2–5 % in the volume. When calculating vibrational properties one is thus faced with the decision, whether one should evaluate the vibrational properties at the theoretically predicted equilibrium lattice constants or at the experimental lattice constants. One can certainly argue in favor of both choices. The first choice (theoretical volume) will guarantee that all sum rules for acoustic branches are properly fulfilled, whereas the second choice might yield results that agree better with experimental values. It is well known that the small error in the predicted equilibrium volume translates into fairly large errors in the elastic properties. The bulk modulus for instance is typically 10% overestimated at the LDA equilibrium volume and 10% underestimated at the GGA volume. Since the elastic moduli are related to the slope of the zone-centered acoustic branches, errors in the elastic moduli will be also visible in the calculated vibrational properties. It is, therefore, expected that calculations at the LDA volume should yield too hard phonons, whereas calculations at the GGA volume should yield too soft phonons. It is remarkable, that despite this argument, LDA based calculations at the LDA volume give the phonon-dispersion relations for the group-IV elemental semiconductors diamond (C),[11] silicon (Si),[12] germanium (Ge),[12] and gray tin (α-Sn) (Ref. 13) in outstanding agreement with experimental findings. This is only partially attributable to scale factors that were introduced for the frequencies, but seems to hinge mostly on a fortuitous but rather systematic error cancellation: by employing the LDA and hence *underestimated* lattice parameters in the phonon calculations good agreement with the experimental findings at *ambient* conditions is obtained for almost all branches. On the other hand, PBE calculations at the PBE lattice constants yield too soft phonon frequencies as first demonstrated for C and Si by Favot and Dal Corso.[14] This was shown to be mostly related to too large theoretical PBE lattice constants.

To remedy the volume errors of LDA and PBE, much effort has been put into the development of "new" *xc* functionals. One such functional is the AM05 functional. It is based on a sub system approach and attempts to fit jellium energies and jellium surface energies (more precisely the airy electron gas).[15] For solids, the functional improves much upon PBE and yields lattice constants that are generally only slightly larger than the experimental values.[16] Subsequently, Perdew modified the PBE functional in order to yield improved surface energies, as well.[17] This so-called PBEsol

functional gives similar lattice constants and surface energies as the AM05 functional.[18]

Another approach reducing the overestimation of lattice constants are hybrid functionals.[19] Hybrid functionals ad-mix a certain amount of nonlocal Hartree-Fock (HF) exchange to a part of local/semilocal LDA/PBE exchange (see Ref. 20 and references 32–41 therein). Since the evaluation of the HF exchange in extended systems, under periodic boundary conditions, requires large computational effort, hybrid functionals have mainly been applied in quantum chemistry. In computational solid state physics, a breakthrough was achieved by Heyd, Scuseria, and Ernzerhof, who proposed the HSE03 functional defined by[21–23]

$$E_{\mathrm{xc}}^{\mathrm{HSE03}} = \frac{1}{4}E_{\mathrm{x}}^{\mathrm{HF,SR}}(\mu) + \frac{3}{4}E_{\mathrm{x}}^{\mathrm{PBE,SR}}(\mu) + E_{\mathrm{x}}^{\mathrm{PBE,LR}}(\mu) + E_{\mathrm{c}}^{\mathrm{PBE}}. \tag{1}$$

The HSE03 functional benefits from the range separation of the HF exchange into a short-(SR) and long-range (LR) contribution and replaces the latter by the corresponding DFT exchange part. The partition into SR and LR parts is defined by the parameter μ and carried out by decomposing the Coulomb kernel according to

$$\frac{1}{r} = S_{\mu}(r) + L_{\mu}(r) = \frac{\mathrm{erfc}(\mu r)}{r} + \frac{\mathrm{erf}(\mu r)}{r}, \tag{2}$$

where erf and erfc are the error and complementary error functions, respectively, and $r=|\mathbf{r}-\mathbf{r}'|$. Thereby, the costly integrals representing the slowly decaying LR HF exchange are avoided and the computational effort reduces significantly. Hybrid functionals have the advantage of increasing the band gap compared to conventional semilocal functionals. We will show below that this can have significant effects on the lattice dynamical properties, in particular in those cases where semilocal functionals incorrectly predict metallic behavior (Sn).

The HSE03 functional,[24] as well as its corrected form the HSE06 functional,[25] have been extensively applied to calculate lattice parameters, bulk moduli, band gaps, and atomization energies of solids including insulators, semiconductors, and metals[26–30] as well as adsorption energies for carbon monoxide on metal surfaces.[31] Izmaylov *et al.* have applied HSE06 and other hybrid functionals to the study of vibrational frequencies of few materials including bulk diamond, two-dimensional hexagonal boron nitride, and organic polymers by analytically evaluating the second energy derivatives with respect to atomic displacements using Gaussian type orbitals.[32,33] To the best of our knowledge, a more comprehensive investigation of the lattice dynamical properties using the HSE06 functional has not been accomplished yet (for $SrTiO_3$ and $BaTiO_3$ see Ref. 34). This motivated us, to apply the HSE06 approach to the calculation of the phonon-dispersion relations of the group-IV elemental solids C, Si, Ge, and α-Sn. The main objective of this work is the comparison of the HSE06 results with LDA, PBE, PBEsol, and experimental findings. The results presented herein are reviewed in the context of previously reported DFT calculations employing the LDA. Particular emphasis is placed on the lattice constants used in the calculations.

II. METHOD OF CALCULATION

The results presented in this work were obtained using the projector augmented wave (PAW) method[35,36] as implemented in the Vienna *ab initio* simulation package (VASP).[37,38] For standard DFT calculations the *xc* energy was treated within the GGA using the parameterization of Perdew, Burke, and Ernzerhof (PBE) (Ref. 5) and its revised form for solids, the PBEsol functional,[17] as well as the LDA (Ref. 4) for the purpose of comparison with previously published calculations. In the present HSE calculations, the HSE06 hybrid functional[25] was applied, where the range-separation parameter μ was set to $\mu=0.207$ Å^{-1} ≈ 0.11 a.u.$^{-1}$ for both, the semilocal as well as the nonlocal part of the exchange functional. From now on, this particular functional will be referred to as HSE.

A. Lattice dynamics from electronic structure theory

The lattice dynamical properties were calculated by a *direct* approach employing the force constant method as outlined in Ref. 39. The key quantity is the interatomic force constant (Hessian) matrix $C(\mathbf{R}_{ni}\alpha,\mathbf{R}_{mj}\beta)$ (Ref. 40) with $\mathbf{R}_{ni}=\mathbf{R}_n+\mathbf{t}_i$ denoting the position of the atoms in the solid at zero temperature. In particular, $\mathbf{R}_n$ ($\mathbf{R}_m$) is the vector connecting different primitive unit cells (PUCs) with n (m) running over all PUCs of the crystal, whereas $\mathbf{t}_i$ ($\mathbf{t}_j$) defines the position of the atom i (j) in the PUC with i (j) running over all atoms in the PUC. The indices α and β label their Cartesian components, respectively. When calculating lattice dynamics from electronic structure theory,[41] the Hessian matrix within the harmonic approximation to the energy[42,43] is given by

$$C(\mathbf{R}_{ni}\alpha,\mathbf{R}_{mj}\beta) = -\frac{\partial F_{\beta}(\mathbf{R}_{mj})}{\partial u_{\alpha}(\mathbf{R}_{ni})}, \tag{3}$$

$$= \frac{\partial^2 E(\{\mathbf{R}\})}{\partial u_{\alpha}(\mathbf{R}_{ni})\,\partial u_{\beta}(\mathbf{R}_{mj})}, \tag{4}$$

where $F_{\beta}(\mathbf{R}_{mj})$ represents the force acting on atom j, when atom i is displaced by $u_{\alpha}(\mathbf{R}_{ni})$ and $E(\{\mathbf{R}\})$ denotes the *Born-Oppenheimer energy surface*. Due to the translational invariance of the crystal, the force constants only depend on the difference $\mathbf{R}_m-\mathbf{R}_n$,

$$C(\mathbf{R}_{ni}\alpha,\mathbf{R}_{mj}\beta) = C_{i\alpha,j\beta}(\mathbf{R}_m-\mathbf{R}_n), \tag{5}$$

and the eigenvectors fulfill a Bloch wave ansatz:

$$\tilde{u}_{i\alpha}(\mathbf{R}_n) = u_{i\alpha}e^{i\mathbf{q}\mathbf{R}_n}. \tag{6}$$

This leads to an implicit definition of the interatomic force constants matrix in reciprocal space

$$C_{i\alpha,j\beta}(\mathbf{R}_m-\mathbf{R}_n) = \sum_{\mathbf{q}} e^{i\mathbf{q}(\mathbf{R}_m-\mathbf{R}_n)}\tilde{C}_{i\alpha,j\beta}(\mathbf{q}). \tag{7}$$

According to the equation of motion $\mathbf{D}(\mathbf{q})\cdot\mathbf{u}(\mathbf{q})=\omega^2\mathbf{u}(\mathbf{q})$, the vibrational eigenfrequencies of the solid are the eigenvalues

$\omega(\mathbf{q})$ of the dynamical matrix $D_{i\alpha,j\beta}(\mathbf{q})$ defined as

$$D_{i\alpha,j\beta}(\mathbf{q}) = \frac{1}{\sqrt{M_i M_j}} \tilde{C}_{i\alpha,j\beta}(\mathbf{q}), \tag{8}$$

where M_i and M_j are the masses of the atoms i and j, respectively. Using this supercell approach only phonon frequencies with wave vectors $\mathbf{q}$ that are commensurate with the supercell dimension are exact. In practice, a finite supercell is used to determine a set of $C_{i\alpha,j\beta}(\mathbf{R}_m - \mathbf{R}_n)$, where $\mathbf{R}_m - \mathbf{R}_n$ is constrained to lie in the Wigner-Seitz cell of the supercell.[44] Phonon frequencies at other $\mathbf{q}$ points are essentially Fourier interpolated. In this work, supercells containing 64 atoms ($2\times2\times2$ conventional cells) were used to evaluate the phonon-dispersion curves.

B. Computational details

The main input to our calculations is the crystal structures of the solids. It is common practice to optimize the lattice constants and internal degrees of freedom before predicting other properties. It is also common practice to neglect zero-point vibration effects. Unfortunately, for lattice dynamical properties, lattice constants have a large effect on the absolute vibrational frequencies, and it is hence not easy to decide which lattice constants one should choose (theory or experiment). As already pointed out, the LDA significantly underestimates the lattice constants, whereas the PBE overestimates the lattice constants by roughly the same amount. In the present work, we aim to compare phonon frequencies evaluated using the HSE functional to the standard local/semilocal LDA/PBE functionals at one specific volume disregarding effects caused by the change of the volume. Thus the lattice constants were chosen to correspond to the lattice constants at which the phonon-dispersion curves were measured. In the case of C and Si, the phonon frequencies have been experimentally determined at ambient conditions only. Accordingly, the room temperature lattice parameters of C and Si were taken from Refs. 45–47. For Ge and α-Sn, the phonon-dispersion curves have been measured at low temperature. Therefore, the lattice constant of natural Ge at 80 K was determined from Ref. 46 as well as from Table 1 in Ref. 48 by taking the values of its isotopes and weighting them with their natural occurrences. In the case of α-Sn, the experimental value measured at 90 K (Ref. 47) was used. The lattice constants and important parameters that determine the accuracy of the VASP calculations are summarized in Table I.

The structural properties and bulk moduli of C, Si, Ge and α-Sn were investigated using $(12\times12\times12)$ Γ-centered $\mathbf{k}$-point meshes corresponding to 72 $\mathbf{k}$ points in the irreducible wedge of the Brillouin zone (BZ). For HSE, the HF exchange energy was evaluated on a $(6\times6\times6)$ mesh.[26] This *downsampling* markedly reduces the computing time. For evaluating the theoretical lattice constants a_0 and the bulk moduli B_0, the volume dependence of the static lattice energy was fitted to a Murnaghan equation of state[49] covering the range $\Omega/\Omega_{eq}=0.94-1.14$, where Ω_{eq} is the experimental equilibrium volume at ambient conditions. In order to avoid effects from the changes in the size of the basis set due to changes in the unit cell volume Ω, the default kinetic energy cutoff E_{cut} has been increased by 25%.

TABLE I. Experimental lattice constants a_0, core radii r_c for the PAW potentials, and kinetic energy cutoffs E_{cut} for the plane wave basis sets are summarized. If the core radii differ for different angular quantum numbers l, they are specified for each l indicated in parenthesis. Nonlocal projectors were generated for the states listed in the column "valence." As local PAW-potential a pseudopotential was generated for the states indicated in the column "local."

	a_0 (Å)	Valence	Local	r_c (a.u.)	E_{cut} (eV)
C	3.5670[a]	$2s2p$	$3d$	1.2(s), 1.5(p,d)	600
Si	5.4310[a]	$3s3p$	$3d$	1.9	400
Ge	5.6524[b]	$4s4p3d$	$4f$	2.2(d)2.3(s,p,f)	600
α-Sn	6.4830[c]	$5s5p4d$	$5f$	2.5	400

[a]Reference 45.
[b]Reference 46.
[c]Reference 47.

Regarding the electronic properties, the following settings were applied. The charge density and wave functions were converged with a uniform $(24\times24\times24)$ Γ-centered $\mathbf{k}$-point mesh. Therefrom the fundamental band gaps were determined and the band structures $E(\mathbf{k})$ were computed on a discrete $\mathbf{k}$ mesh along high symmetry directions in the BZ, i.e., from the L point with the reciprocal coordinates (0.5,0.5,0.5) to the BZ center Γ (0,0,0) and the X point (0,0,1) in units of $2\pi/a$.

For the calculation of the phonon-dispersion curves, the Brillouin zone integrations were carried out on symmetry reduced Monkhorst-Pack[50] $(4\times4\times4)$ $\mathbf{k}$-point grids using the Gaussian smearing method with 50 meV smearing width. In the case of HSE calculations, a $(2\times2\times2)$ $\mathbf{k}$-point grid was applied and the $\mathbf{k}$-point grid for the evaluation of the short-range HF operator was further reduced by a factor of 2 according to Ref. 26. Convergence tests of the zone-center phonon frequencies with respect to the $\mathbf{k}$-point grid showed that for the applied supercells an accuracy of 0.005 THz is achieved with the given meshes. For α-Sn, the uncertainty of the highest optical zone-center phonon frequency is 0.05 THz (0.008 THz) for PBE (HSE) with these settings. For the electronic self-consistency loop a total energy convergence criterion of 1.0×10^{-7} eV was applied to assure highly converged forces.

III. RESULTS AND DISCUSSION

In order to obtain a precise description of the lattice dynamical properties, theory should be able to yield both, the structural and the electronic properties of the materials with high accuracy. To evaluate the accuracy of the applied functionals for simpler ground state properties, the theoretical lattice parameters a, bulk moduli B_0 as well as band structures were calculated using the PBE and the HSE functional.

A. Lattice constants and bulk moduli

In Table II the results on the structural and elastic properties are summarized and compared to previously reported

TABLE II. The optimized theoretical lattice constants a (Å) and bulk moduli B_0 (GPa) calculated using different xc functionals (LDA, PBE, PBEsol, and HSE) are compared to previously reported values from first-principles calculations with local basis sets (GTO), the full-potential linearized augmented plane wave (FP-LAPW) method, as well as the norm-conserving pseudopotentials (NC-PP) and experimental findings (Ref. 45). The relative error compared to experiment for the calculated lattice constants is given in parentheses. Zero point vibration corrections have not been applied.

	LDA		PBE		PBEsol		HSE		EXPT.[a]	
	a	B_0	a	B_0	a	B_0	a	B_0	a_0	B_0
C										
PAW[b]	3.538(−0.8%)	466	3.574(+0.2%)	431	3.557(−0.3%)	451	3.549(−0.5%)	467	3.567	442
GTO[c]	3.537(−0.8%)	454	3.579(+0.3%)	422			3.553(−0.4%)	458		
LAPW[d]	3.536(−0.9%)	469	3.575(+0.2%)	434	3.557(−0.3%)					
NC-PP[f]	3.530(−1.0%)	473								
Si										
PAW[b]	5.413(−0.3%)	96	5.469(+0.7%)	88	5.436(+0.1%)	93	5.435(+0.1%)	98	5.431	94.8–
GTO[c]	5.410(−0.4%)	95	5.479(+0.9%)	89			5.444(+0.2%)	99		99
LAPW[d]	5.407(−0.4%)	96	5.475(+0.8%)	89	5.438(+0.1%)					
NC-PP[f]	5.398(−0.6%)									
Ge										
PAW[b]	5.627(−0.5%)	73	5.760(+1.8%)	58	5.674(+0.3%)	67	5.682(+0.4%)	71	5.657	73.6–
GTO[c]	5.634(−0.4%)		5.776(+2.1%)				5.701(+0.8%)			74.9
LAPW[d]	5.625(−0.6%)	73	5.763(+1.9%)	60	5.678(+0.4%)					
NC-PP[f]	5.609(−0.8%)									
α-Sn										
PAW[b]	6.481(−0.2%)	45	6.657(+2.6%)	35	6.542(+0.8%)	42	6.561(+1.1%)	43	6.491	54.6
LAPW[d]	6.473(−0.3%)	46	6.655(+2.5%)	36	6.540(+0.8%)					
PAW(SOC)[e]			6.659(+2.6%)	35						
NC-PP[f]	6.38(−1.7%)									

[a]Experimental values at ambient conditions from Reference 45.
[b]This work using the LDA, PBE, PBEsol, or the HSE06 functional.
[c]From References 52 and 23 using the PBE or the HSE03 functional.
[d]From References 51 and 53 using the LDA, PBE, and PBEsol functional.
[e]This work using the PBE functional and taking into account spin-orbit coupling (SOC).
[f]LDA values from References 11–13.

results from first-principles calculations, as well as experimental findings. We first note that the present results agree very well with full-potential (FP) linearized augmented plane wave (LAPW)[51] and Gaussian-type orbital (GTO) results published before. For comparison, also the lattice constants for the norm-conserving pseudopotentials, which were used in the previous phonon calculations, are summarized from Refs. 11–13. Due to the neglect of core-valence interactions (nonlinear core effects in the exchange and correlation), the norm-conserving pseudopotentials (NC-PP) underestimate the lattice constants with severe and unacceptably large errors for α-Sn, pointing toward some deficiency of the NC Sn potential. We will return to this issue later.

When analyzing the results presented in Table II the following—meanwhile widely manifested—trends are observed. First, for all studied materials, PBE overestimates the lattice constants resulting in an underestimation of the bulk moduli. This underestimation of the bulk modulus is one order of magnitude larger than the overestimation of the lattice constant emphasizing the high sensitivity of the former to the volume. When focusing on the PAW-PBE lattice constants in Table II, a significant increase of the relative error compared to experiment is observed within the series. While for C and Si the lattice constants deviate less than 1% from the experimental value, the discrepancy is 1.8% and 2.6% for Ge and α-Sn, respectively. The resulting errors in the bulk moduli increase from roughly 3% (C) to 35% (α-Sn) in the group-IV series. This can be explained by the presence of semicore d electrons that are not well described using PBE in the latter two materials.

Interestingly, an analysis of the PAW-LDA values reveals that LDA yields too small lattice parameters but is more consistent than PBE with a smaller relative increase of the lattice constants along the series. Furthermore, inclusion of zero-point vibration effects in a simple Debye model, increases the theoretical lattice constants by 0.6%, 0.2%, 0.2% and 0.15% for C, Si, Ge and Sn,[53] yielding lattice constants within 0.3% for group-IV solids. This is, in fact, a remarkable performance, not achieved by the other functionals.

The HSE functional generally decreases the lattice constants compared to PBE. The reduction is small for C and Si (0.6%), but fairly large for Ge and α-Sn (1.5%), which is

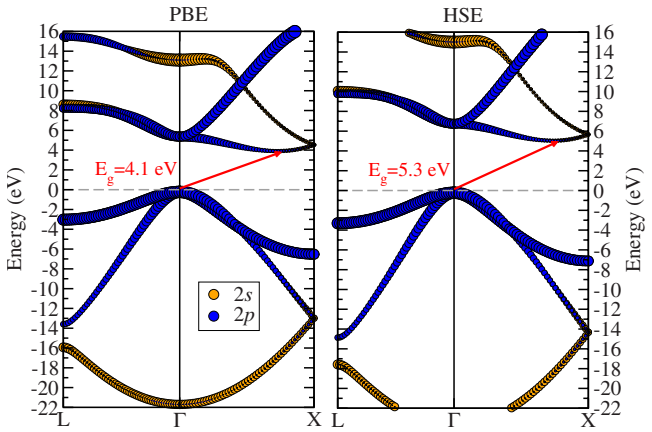

FIG. 1. (Color online) PBE and HSE band structures of diamond along $\overline{L\Gamma X}$. The band character is indicated by circles, where the size correlates with the amount of s and p character, respectively. The top of the valence band is marked by the dashed line. The fundamental electronic gap is indicated by the arrow.

most likely related to a contraction of the $3d$ and $4d$ shell when going from PBE to HSE. Without zero-point vibration corrections, the HSE functional slightly underestimates the lattice constant of C, but overestimates it for the other materials, and the error increases again with increasing mass. After inclusion of zero-point vibration effects (0.6%, 0.2%, 0.2% and 0.15% for C, Si, Ge and Sn) (Ref. 53) the HSE lattice constants for C and Si are in excellent agreement with experiment, whereas those of Ge and α-Sn are roughly 0.5% and 1.3% too large.

Remarkably, the PBEsol functional yields similar results as the HSE functional. For C, the lattice constant is slightly larger than for the HSE approach, whereas for Ge and α-Sn it is 0.2% smaller than for HSE. For PBEsol, the bulk moduli are consistently softer than for HSE and therefore in slightly worse agreement with experiment than for HSE. This suggests a slightly softer effective interatomic potential, which is confirmed below, with PBEsol predicting smaller phonon frequencies than HSE.

In the case of α-Sn, we also studied the importance of spin-orbit coupling (SOC). The PBE volume optimization

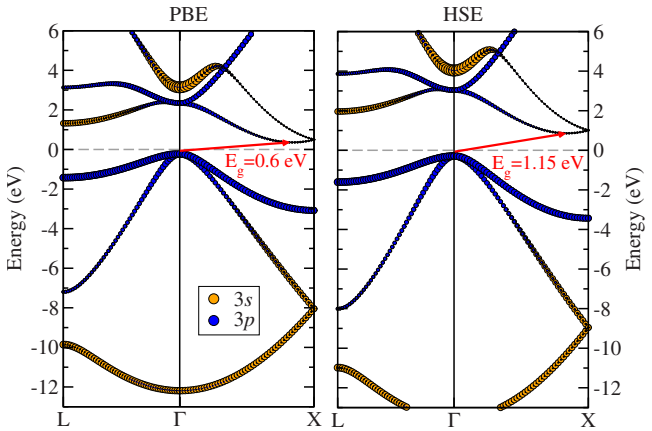

FIG. 2. (Color online) Analogous to Fig. 1: band structures of silicon.

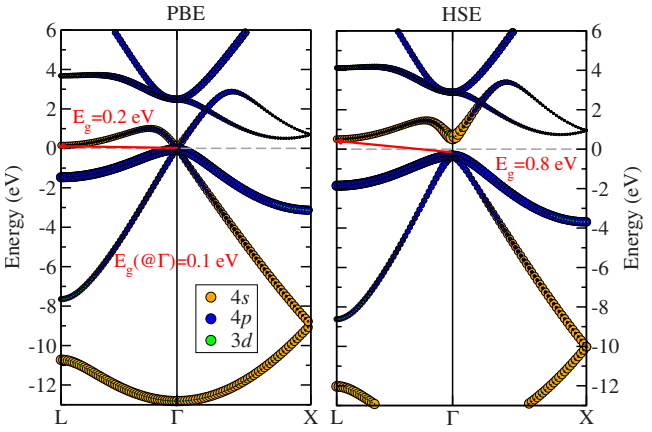

FIG. 3. (Color online) Analogous to Fig. 1: band structures of germanium.

revealed that including relativistic effects for the valence electrons causes only minor changes in the structural and elastic properties.

B. Band structures and gaps

The band structures of the entire series are depicted in Figs. 1–4, and the band gaps are summarized in Table III. Although all group-IV elements have an s^2p^2 valence electron configuration, the materials exhibit quite different electronic properties. Within the series, the valence s orbitals move down in energy compared to the total bandwidth of the valence band. The lowering of the s shell (compared to the bandwidth) is for instance visible in the almost constant s-p energy separation of 3 eV at the L point throughout the series. It is a result of relativistic effects and the occupation of the $3d$ shell in Ge and $4d$ shell in Sn. The progressive lowering of the valence s shell determines all trends across the series. (i) The tendency toward the formation of sp^3 hybrid orbitals becomes weaker along the series and resultantly the metallicity increases: α-Sn easily transforms to the metallic β-Sn with a crystal structure intermediate between diamond and the face centered cubic structure, and lead (Pb) is a metal. (ii) The conduction band is dominated by s and p like

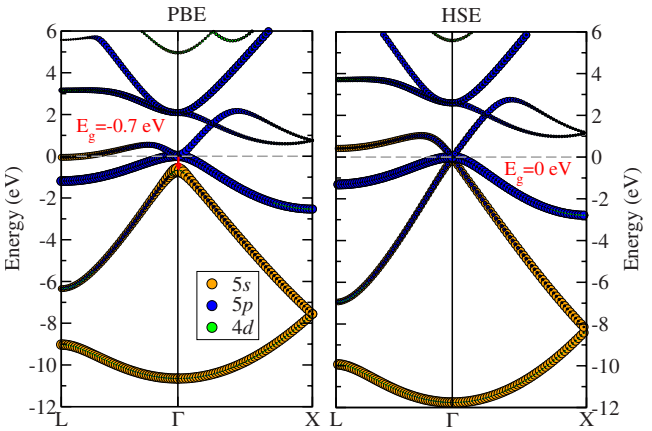

FIG. 4. (Color online) Analogous to Fig. 1: band structures of α-Sn. Fermi-level is marked by the dashed line.

TABLE III. PBE and HSE fundamental electronic band gaps as well as direct band gaps evaluated at the Γ-point in (eV) compared to experimental findings (Refs. 42, 45, and 54). The abbreviation "ind" points out that the fundamental gap is *indirect*.

	PBE		HSE		EXPT.	
(eV)	E_g (ind)	E_g (Γ)	E_g (ind)	E_g (Γ)	E_g (ind)	E_g (Γ)
C	4.13	5.59	5.26	6.98	5.46–5.60	7.3–7.4
Si	0.58	2.57	1.15	3.33	1.12	3.40
Ge	0.21	0.09	0.85	0.94	0.66	0.81
Ge (SOC)			0.71	0.77	0.66	0.81
α-Sn		−0.67		0		0–0.10

antibonding hybrid orbitals. With the lowering of the valence *s* orbital, also the antibonding *s* states move down in energy. In C and Si, the bottom of the conduction band has predominant *p*-like character, whereas in Ge and Sn, *s* orbitals dominate the bottom of the conduction band. Matter of fact, this again goes hand in hand with an increasing metallicity. Additionally, the occupation of the 3*d* and 4*d* states affects details of the conduction bands, with increasing *d* character for Ge and Sn.

PBE fails to reproduce the correct band order in Ge and suggests a direct fundamental band gap located at Γ instead of the indirect gap with the valence band maximum (VBM) located at Γ and the conduction band minimum (CBM) at *L*. Moreover, it yields a metallic ground state solution (negative energy gap) for α-Sn. HSE corrects these shortcomings and provides the right ground state solutions and band structures for all materials within the series.

Concerning the energy gaps summarized in Table III, PBE severely underestimates the indirect fundamental energy gaps for C, Si, and Ge, as well as the direct gaps at the Γ-point. Similar observations are made for PBEsol (not shown), which predicts band gaps that are typically 0.05 eV smaller than the PBE values. The errors of semilocal functionals are well-known to be related to (i) the incomplete cancellation of self-interaction within the valence band resulting in too shallow valence electrons and (ii) the complete absence of the discontinuity of the derivative of the *xc* potential with respect to the number of electrons. HSE also lacks an integer discontinuity, but due to the nonlocal screened exchange operator the HSE one-electron gaps compare well with experiment. In the case of Ge, the HSE gaps are too large, as long as SOC is neglected. Inclusion of SOC, however, brings the results again within 5% of experiment. Remarkably, using HSE the zero-gap semiconducting ground state of α-Sn is well reproduced.

C. Phonon-dispersion relations

1. Carbon

In the following, the phonon-dispersion relations of the group-IV elemental solids calculated with different *xc* functionals are discussed. Phonon frequencies of the transversal and longitudinal acoustic (TA/LA) and optical (TO/LO) modes, respectively, at selected high symmetry points are given in Table IV together with experimental findings[55–59] and previously reported DFT calculations using norm-conserving pseudopotentials and density functional perturbation theory.[11–13] In the present investigation, accurate PAW potentials and the supercell approach with 64 atoms in cubic supercells were applied ($4\times4\times4$ **k**-points).

For the reasons outlined in Sec. II B, *volume effects* are investigated on the level of LDA first (see Fig. 5). To this end, we have calculated the dispersion relation at the experimental ambient equilibrium lattice constant (a_0=3.567 Å) and at the theoretical LDA lattice constant (a=3.5296 Å, without zero-point corrections, which increase the theoretical lattice constant of diamond by 0.6%). This choice was motivated by the observation, that the previously published NC-PP LDA calculations[11–13] have been performed at the LDA lattice constant. We however also note that Ref. 43 points out that the calculated data for C have been rescaled for the comparison to the experimental phonon frequencies at room temperature.

As a result of the small LDA volume, the phonon frequencies are larger than those obtained from LDA calculations at the experimental a_0 as demonstrated in Fig. 5. The volume effect is particularly pronounced for the optical branches, e.g., the zone-center optical mode $\Gamma_{LO/TO}$ is roughly 1.3 THz larger at the LDA lattice constant than at the experimental a_0. For this reason and also due to the previously mentioned scaling, perfect agreement between theory and experiment had been claimed in Refs. 11 and 43. This, however, is deceiving without denying that a tendency for error compensation exists in the LDA. LDA predicts too small volumes, and at these too small volumes many vibrational frequencies agree exceptionally well with experiment. However, even this cancellation cannot be universal. At the LDA volume elastic moduli are usually 5–10 % too large compared to experiment (see Table II), and since the elastic moduli correspond to a linear combination of the slopes of the acoustic phonon branches around Γ, the slopes cannot agree well with experiment. Admittedly, a 5% error in some acoustic branches will be hardly noticeable in the way phonon-dispersion relations are usually presented, but evaluation at the experimental volume should reduce these errors.

Furthermore, inclusion of zero-point vibration corrections for the volume will also require one to increase the lattice constant by 0.6% worsening agreement with experiment. For the remainder of the work, we have therefore decided to stick in most cases to the experimental lattice constants, well aware of the fact that this leads to a violation of sum rules, since the external pressure is nonzero. To determine whether and how differences in the potentials might be responsible for differences to previous publications, we have determined the phonon frequencies at the LDA volume using LDA PAW potentials for selected cases as well. In addition, HSE phonon frequencies at theoretical HSE volumes (without zero-point vibration corrections) are presented for all considered materials, in order to test the quality of this functional without resorting to any experimental parameters (the experimental lattice constants in this case). Table IV indicates that the potentials make little difference for diamond with discrepancies being smaller than 0.4 THz (13 cm^{-1}, see Table IV rows NC-PP LDA and PAW LDA).

TABLE IV. Calculated phonon frequencies of group-IV elemental solids at high symmetric points in comparison with experiment (Refs. 55–59) and previously reported DFT calculations using norm-conserving pseudopotentials (NC-PP) and density functional perturbation theory (Refs. 11–13). All values are given in THz. The lattice constant used for the particular calculation is given in the second column.

(THz)	a (Å)	$\Gamma_{LO/TO}$	X_{TA}	$X_{LA/LO}$	X_{TO}	L_{TA}	L_{LA}	L_{LO}	L_{TO}
C									
NC-PP LDA[a]	3.530	39.7	24.0	36.8	32.8	16.8	32.4	38.2	36.9
PAW LDA	3.530	39.9	23.6	36.7	33.1	16.5	32.4	37.9	37.1
PAW LDA	3.567	38.6	23.4	35.7	31.6	16.4	31.1	37.3	35.7
PAW PBEsol	3.567	38.9	23.2	35.8	32.1	16.2	31.5	37.2	36.1
PAW PBE	3.567	39.0	23.4	35.9	32.1	16.4	31.5	37.4	36.1
PAW HSE	3.567	40.4	24.0	36.8	32.9	16.7	32.1	38.4	37.3
PAW HSE	3.549	41.0	24.1	37.3	33.6	16.8	32.7	38.7	37.9
EXPT.[b]	3.567	40.3	24.2	36.1	32.6	16.4	31.0	37.2	36.3
Si									
NC-PP LDA[c]	5.398	15.5	4.4	12.4	14.0	3.3	11.3	12.6	14.8
PAW LDA	5.431	15.2	4.2	12.1	13.6	3.2	11.1	12.1	14.4
PAW PBEsol	5.431	15.3	4.0	12.2	13.7	3.1	11.1	12.3	14.6
PAW PBE	5.431	15.4	4.2	12.3	13.8	3.2	11.2	12.4	14.6
PAW HSE	5.431	15.9	4.7	12.6	14.1	3.5	11.6	12.7	15.1
PAW HSE	5.435	15.8	4.7	12.6	14.0	3.5	11.6	12.5	15.0
EXPT.[d]	5.431	15.5	4.5	12.3	13.9	3.4	11.4	12.6	14.7
Ge									
NC-PP LDA[c]	5.609	9.17	2.40	7.28	8.24	1.86	6.72	7.34	8.72
PAW LDA	5.652	8.71	2.33	6.97	7.85	1.90	6.50	6.97	8.31
PAW PBEsol	5.652	8.78	2.20	7.02	7.97	1.81	6.48	7.09	8.40
PAW PBE	5.652	8.91	2.14	7.12	8.14	1.79	6.51	7.27	8.55
PAW HSE	5.652	9.16	2.40	7.29	8.26	1.85	6.74	7.37	8.74
PAW HSE	5.682	9.01	2.43	7.16	8.07	1.85	6.68	7.17	8.57
EXPT.[e]	5.652	9.11	2.40	7.22	8.27	1.89	6.66	7.34	8.69
α-Sn									
NC-PP LDA[f]	6.38	5.9	1.2	4.7	5.5	1.1	4.2	4.9	5.7
PAW LDA	6.38	5.83	1.05	4.83	5.86	1.01	4.16	5.19	5.99
PAW LDA	6.483	5.45	1.23	4.56	5.45	1.10	4.01	4.78	5.62
PAW PBEsol	6.483	5.51	1.08	4.60	5.55	1.02	4.01	4.88	5.70
PAW PBE	6.483	5.70	0.94	4.68	5.68	0.95	4.04	5.03	5.82
PAW HSE	6.483	6.10	1.10	4.75	5.73	0.86	4.19	5.06	5.92
PAW HSE	6.561	5.86	1.21	4.56	5.42	0.92	4.11	4.77	5.65
EXPT.[g]	6.483	6.0	1.3	4.7	5.5	1.0	4.2	4.9	5.7

[a]LDA values from Reference 11.
[b]Experimental values measured at 296 K from Reference 55.
[c]LDA values from Reference 12.
[d]Experimental values measured at 300 K from References 56 and 57.
[e]Experimental values measured at 80 K from Reference 58.
[f]LDA values from Reference 13.
[g]Experimental values measured at 90 K from Reference 59.

In Fig. 6 the calculated phonon-dispersion relation of diamond is compared to experimental data.[55,60–62] Compared to the LDA results shown in Fig. 5, the phonon frequencies obtained with PBE are higher at the experimental volume and in reasonable agreement with experiment. The PBEsol values are generally between the LDA and the PBE values,

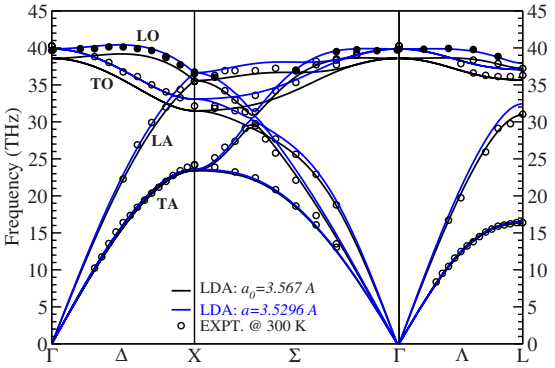

FIG. 5. (Color online) Phonon-dispersion relations $\omega(\mathbf{q})$ of C calculated using LDA along the path $\Gamma-X-K-\Gamma-L$. This path corresponds to the $\mathbf{q}$ directions Δ ($\Gamma-X$ or [100]), Σ ($\Gamma-K-X$ or [110]), and Λ ($\Gamma-L$ or [111]). The LDA phonon modes were calculated at the experimental equilibrium lattice constant a_0 =3.567 Å and at the LDA optimized one (a=3.5296 Å) taken from Ref. 11. The experimental values have been taken from Ref. 55 (open symbols) and Ref. 60 (full symbols) and were measures at ambient conditions (a_0=3.567 Å).

but closer to the PBE results, except for the transverse acoustic branches (X_{TA},L_{TA}) that are softer than for PBE *and* LDA using PBEsol. The same is observed for Si (see below).

HSE, on the other hand, increases the phonon frequencies, in particular, those of the optical modes, which are related to ions moving out of phase within one unit cell. The stiffening of the optical modes is almost constant throughout the entire Brillouin zone, pointing toward an increased nearest-neighbor interaction due to the inclusion of nonlocal HF exchange. The agreement with experiment is good for both PBE and HSE. On average, HSE yields slightly too high frequencies in particular close to the L point (compare Table IV), whereas PBE underestimates the frequencies, in particular for the $\Gamma_{LO/TO}$ and $X_{TA/TO}$ modes. PBEsol results are lying between LDA and PBE, resulting in a slightly more pronounced underestimation of the frequencies than for PBE.

For completeness, we have also included the HSE frequencies at the theoretical HSE volume (not corrected for zero-point vibration effects). Since zero-point vibration effects increase the volume by 0.6% for C,[53] bringing about

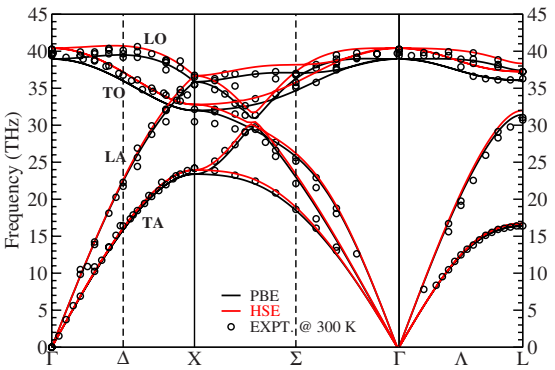

FIG. 6. (Color online) Phonon-dispersion relations $\omega(\mathbf{q})$ of C calculated with PBE and HSE. The experimental values have been taken from Refs. 55 and 60–62.

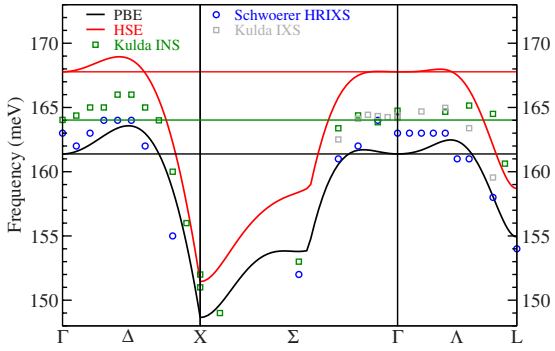

FIG. 7. (Color online) LO branch of diamond calculated with PBE and HSE along Δ, Σ, and Λ in comparison to INS data of Kulda *et al.* (Ref. 63) more recent IXS data of Kulda *et al.* (Ref. 60), and HRIXS data of Schwoerer-Böhning *et al.* (Ref. 61). The horizontal lines indicate the Γ-point optical phonon frequencies, respectively.

perfect agreement with the experimental volume, we only comment that a decrease of the volume increases the phonon frequencies by 2%, which would worsen agreement with experiment further. However, because zero-point vibration effects should be included in the theoretical volume, these results are not particularly relevant.

Within the series, diamond exhibits one unique feature in the phonon-dispersion relation, the overbending of the uppermost longitudinal optical (LO) branch: the phonon-dispersion maximum is not located at the Γ point. Concerning the magnitude of this overbending (only a few meV) and the $\mathbf{q}$ direction where it appears, different experiments, such as inelastic neutron scattering (INS),[63] inelastic X-ray scattering (IXS),[60] and high resolution IXS (HRIXS) (Ref. 61) as well as *ab initio* calculations[64,65] give contradictory results. It is generally argued that the dispersion maximum of the LO mode slightly above the zone-center optical phonon frequency ω_0 causes a peak in the one-phonon density of states (DOS). The latter is also projected onto the two-phonon DOS at a frequency above $2\omega_0$ and tentatively explains the experimentally observed anomalous maximum in the second-order Raman spectrum of diamond at an energy that is roughly 25 cm^{-1} (3 meV) greater than twice ω_0.[64] A prerequisite for the appearance of this peak is that the LO branch has a minimum at Γ. This in turn requires the optical phonon mode to exhibit an overbending in *all* $\mathbf{q}$ directions. If the LO branch has a saddle point at Γ, the peak in the second-order Raman spectrum would be located exactly at $2\omega_0$, whereas a maximum would not result in any peak.[64] The origin of this overbending can be traced back to the bond-bending forces being stiffer in diamond than in other tetrahedrally bonded semiconductors due to more tightly bound sp^3 hybridized electrons. This leads to particularly strong effective second-nearest neighbor forces.[60] An alternative interpretation of the peak in the second-order Raman spectrum relies on an anomaly in the bond polarizability without invoking any special features in the phonon spectrum.[66] In order to resolve this issue, we focus on the LO mode and evaluated our data with respect to the overbending as shown in Fig. 7 and Table V. For this analysis the phonon calculations were repeated using a $(4\times4\times4)$ supercell containing 512 atoms to be able

TABLE V. Overbending of the LO branch in diamond (meV) along the **q** directions Δ, Σ, and Λ.

(meV)	Δ	Σ	Λ
NC-PP LDA[a]	2.5–3.2	1.0–1.4	1.4–1.8
PAW LDA	2.4	0.5	1.3
PAW PBE	2.2	0.3	1.1
PAW HSE	1.2	0.0	0.2
EXPT. HRIXS[b]	1.2	0	0
EXPT. INS[c]	1.5 ± 0.3		
EXPT. IXS[d]	0.9–1.9	0.2	0.4–0.6

[a]DFPT NC-PP calculations using LDA as described in References 11 and 64. Values are taken from Table I in Reference 63 and Table I in Reference 60.
[b]High resolution inelastic x-ray scattering data from Reference 61.
[c]Inelastic neutron scattering data from Reference 63.
[d]Inelastic x-ray scattering data from Table I in Reference 60.

to capture fine details in the dispersion relation. The LDA/PBE calculations suggest an overbending in all three directions. The overbending is most pronounced along Δ (2.5 meV) and still sizable along Λ (1 meV). Except for Σ our values agree very well with NC-PP LDA calculations.[11,64,63] The remaining small discrepancies might be related to different pseudopotentials (1 meV according to Ref. 63), or different volumes (unlikely according to our test calculations) or the supercell approximation we have used.

In comparison to experiment, the main issue is that the LDA and PBE values are significantly larger then the experimental estimates of 1.5 ± 0.3 meV (Δ) and 0.4–0.6 meV (Λ), respectively. Moreover, the maximum along Δ (Λ) appears at larger **q** (smaller **q**) than experimentally observed. The HSE calculations clearly yield a much reduced overbending along Δ (1.2 meV), resulting in very good quantitative agreement with the INS as well as IXS data of Kulda *et al.*[60,63] Furthermore, the location of the maximum is close the experimentally observed one. For Σ and Λ, the HSE values are also significantly reduced compared to the PBE values (again typically by 1 meV), such that the overbending becomes very small (0.2 meV) along Λ and negligible along Σ. This essentially agrees with the experimental observations.

In conclusion, the HSE calculations presented in this work suggest that the LO phonon branch exhibits a very weak minimum at Γ, with negligible overbending along Σ. Semilocal functionals clearly overestimate the overbending by about 1 meV. The experimentally observed values[60,61,63] are consistent with our prediction, but the experimental spread and the precision of our present calculations are not quite sufficient to entirely confirm or exclude an overbending along Σ. It is however certain, that hybrid functionals reduce the overbending by about 1 meV yielding better overall agreement with experiment.

2. Silicon

Within the group-IV elemental solids, Si represents the most "ideal" semiconductor. In Fig. 8 the calculated lattice dynamics are compared to experiment.[56,57,67] In contrast to

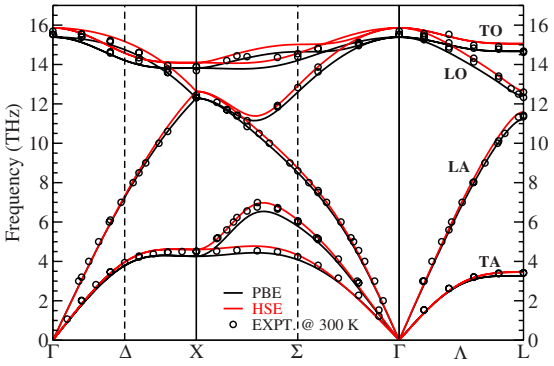

FIG. 8. (Color online) Analogous to Fig. 6: phonon-dispersion relations $\omega(\mathbf{q})$ of Si calculated within PBE and HSE along the **q** path Γ–X–K–Γ–L. The experimental values have been taken from Refs. 56, 57, and 67.

C, the highest optical mode is the transversal one. As for C, PBE and PBEsol yield almost identical results, except for the transverse acoustic branches (X_{TA}, L_{TA}) which are again too soft for PBEsol. The differences between PBE and HSE are also very similar as for C diamond, with HSE yielding greater phonon frequencies than PBE. Except for a slight underestimation of the LO and TO branches as well as the TA branches, the PBE lattice dynamics agree quite well with the experimental findings. The HSE functional overcorrects and slightly overestimates the frequency of the optical modes throughout the entire Brillouin zone. On the other hand, a noticeable improvement for the TA modes along Σ is achieved. As the theoretical HSE lattice constant is close to the experimental one, the influence of the choice of the lattice constant on the phonon frequencies (theory or experiment) is negligible for Si. As for C, PBEsol yields phonon frequencies between PBE and LDA, again with the exception of the TA modes, which become much too soft.

In summary, PBE and HSE yield reasonable results at the experimental volume, with HSE having a tendency toward overestimation and PBE a slight tendency for underestimation. The underestimation is more pronounced in PBEsol and even stronger in LDA.

3. Germanium

The phonon spectrum of Ge is presented in Fig. 9. The improvement from PBE to HSE is a little bit more evident for Ge (and rather profound in α-Sn, see below). As already pointed out in Sec. III B, HSE is able to yield the correct electronic band structure for these solids and we believe that this is eventually the main reason why HSE gives a better description of the phonon modes than PBE. PBE again underestimates the highest frequency optical branches and HSE raises the frequencies in particular at the Γ point ($\Gamma_{\mathrm{LO/TO}}$) bringing about better agreement with the experimental dispersion relation. The improvement by HSE is also significant for the transversal acoustic branches TA1 and TA2 throughout the spectrum thus yielding excellent agreement with experiment. Evaluating the HSE phonon dispersion at the theoretical HSE lattice constant leads to slightly smaller frequencies for the optical modes (but still in good agree-

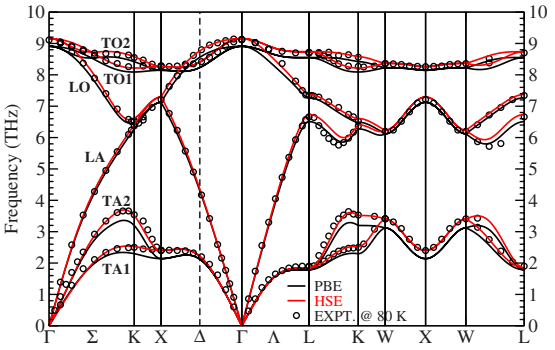

FIG. 9. (Color online) Phonon-dispersion relations $\omega(\mathbf{q})$ of Ge calculated within PBE and HSE along the $\mathbf{q}$ path $\Gamma-X-K-\Gamma-L-K-W-X-W-L$. The experimental values measured at 80 K have been taken from Ref. 58.

ment with experiment), while the acoustic branches remain effectively unchanged. Again PBEsol yields phonon frequencies in between LDA and PBE, and usually the frequencies follow the order PBE>PBEsol>LDA. Only for the TA branches at X and L, this order is reversed (LDA>PBEsol>PBE).

Note that the Ge calculations correspond to the low temperature lattice constant (80 K), since the vibrational frequencies were measured at this temperature. To complement these results, we also performed calculations at the room temperature lattice constant (as done before for C and Si), and found somewhat different changes from PBE to HSE. At the room temperature lattice constant, changes in the frequencies of the longitudinal acoustic (LA) modes were minor from PBE to HSE, and only the LO and TO branches increased from PBE to HSE. This is very similar to the results for C and Si, and indicates that even small changes in the lattice constant can have a dramatic impact on the results and how the functional affects the phonon frequencies.

4. α-Tin

For α-Sn, our present PBE calculations yield results of moderate quality only (see Fig. 10). This is astonishing, since the previous NC-PP calculations gave virtually perfect agreement with experiment. We therefore first determined whether the former good agreement was related to the use of the LDA volume. However, with the PAW technique we were not able to reproduce the NC-PP α-Sn results even at the LDA volume (compare Table IV). Generally the PAW method yields harder frequencies for the optical modes at the X and L point, whereas at the Γ point similar results as for the NC-PP calculations are found. This, however, implies that the dispersion along ΓX and ΓL is qualitatively wrong (flat) and similar to the PBE results at the experimental volume (see Fig. 10). We carefully tested a number of different PAW potentials to be certain that our results are technically well converged. Also note that the excellent accuracy of the PAW potentials was already confirmed by the comparison with the LAPW lattice parameter and bulk modulus in Table II, and indeed we found the results to be robust with respect to the PAW parameters. This indicates that the previous agreement between theory and experiment was fortuitous and cannot be reproduced using state of the art techniques: converged LDA or PBE calculations do not agree with the experimentally measured phonon-dispersion relation and predict a qualitatively incorrect dispersion for the optical branches. At the Γ point, the TO and LO modes are too soft, and the acoustic modes show anomalous dispersion at X, as well. One possible explanation of the observed softening is a coupling between the states at the Fermi-level and the Γ-point phonons. To confirm this conjecture, we performed one calculation with the $4d$ electrons in the core and sampling the Brillouin zone at a single special $\mathbf{k}$-point $(0.25,0.25,0.25)\,2\pi/a$. With this setup, Sn became artificially insulating (Γ point is avoided), and indeed the phonon frequencies agreed now reasonably with experiment (and the previous NC-PP calculations). This confirms our conjecture: the incorrect electronic band order at Γ in LDA/PBE causes the observed phonon softening at Γ.

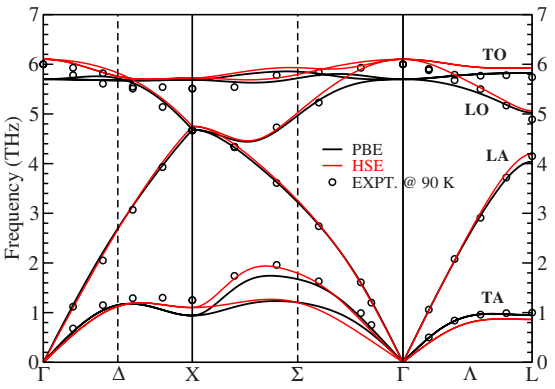

FIG. 10. (Color online) Analogous to Fig. 6: phonon-dispersion relations $\omega(\mathbf{q})$ of α-Sn calculated within PBE and HSE along the $\mathbf{q}$ path $\Gamma-X-K-\Gamma-L$. The experimental values measured at 90 K have been taken from Ref. 59.

The HSE functional repairs these deficiencies by restoring a semimetallic behavior. Accordingly it yields the correct dispersion relation for the optical branches, even in the limit of many $\mathbf{k}$ points. Furthermore the description of the acoustic modes is much improved at the X point (but worsens slightly at the L point). Since the difference between the theoretical HSE and experimental lattice constants is 1.1% for α-Sn, the phonon modes become significantly softer at the theoretical lattice constant. While the optical phonon frequencies were overestimated at the experimental lattice constant, they are underestimates at the theoretical volume. On the other hand, the frequencies of the acoustic modes increase with the lattice constants, yielding better agreement with experiment at the theoretical HSE lattice constant. Hence overall, the HSE results at the theoretical HSE lattice constant are in even better agreement with experiment than at the experimental lattice constant.

The changes from PBE to PBEsol are almost identical to Ge, with the PBEsol frequencies lying between the LDA and PBE values. Again, the frequencies usually increase from LDA over PBEsol to PBE, with the exception of the TA modes, which become softer from LDA over PBEsol to PBE.

IV. DISCUSSION

In this work, the HSE hybrid functional has been used to calculate the lattice dynamical properties of the group-IV

elemental solids including diamond, silicon, germanium, and gray tin. The results have been compared to local and semilocal density functionals, LDA, PBE and PBEsol, to previous calculations and to experimental findings. Regarding the structural, elastic and electronic properties of these materials, HSE yields results superior to LDA and PBE, in particular, for Ge and α-Sn, which both possess semicore d electrons. The lattice constants, bulk moduli, as well as the band gaps are in good agreement with experiment in contrast to PBE, which severely (i) overestimates the lattice constants, (ii) underestimates the bulk moduli, (iii) underestimates the band gaps, and (iv) incorrectly predicts a metallic ground state for α-Sn. Except for the band gaps, which remain on the PBE level, PBEsol predicts remarkably similar structural properties as HSE.

For the lattice dynamics, we have emphasized that good but fortuitous agreement with experiment can be achieved by choosing LDA optimized lattice constants and by comparing to experimental data measured at ambient conditions. LDA underestimates the volume, and LDA also underestimates the vibrational frequencies. Both effects seem to cancel to some extent, i.e., by evaluating the vibrational frequencies at a smaller volume than considered experimentally reasonable agreement with experiment is often found.

If the vibrational frequencies are evaluated at one specific volume, we find that the phonon frequencies of the optical branches increase from LDA, over PBEsol to PBE. Among the three semilocal functionals, PBE yields the best agreement with experiment at the experimental volume, with a slight tendency toward too soft frequencies, confirming a similar trend already observed for $BaTiO_3$ or $SrTiO_3$.[34] The hybrid HSE functional increases the vibrational frequencies even further, resulting in an overestimation of the vibrational frequencies which is most pronounced for the optical modes. The overestimation is rather constant throughout the entire Brillouin zone, pointing toward too stiff nearest-neighbor interactions. With the exception of α-Sn, the overall agreement with experiment is already exceptionally good at the PBE level. The only issue is that such calculations at the experimental volume induce a significant pressure, since the PBE functional overestimates the lattice constants significantly. Unfortunately, the PBEsol functional, which predicts more accurate lattice constants than PBE, tends to underestimate the vibrational frequencies. We are therefore left with the slightly troublesome result that the two functionals that predict the best equilibrium volumes either underestimate (PBEsol) or overestimate (HSE) the vibrational frequencies. A hybrid functional using PBEsol for the local part of the exchange and correlation energy might solve this problem.

Although, changes from PBE to HSE are generally only qualitative, for α-Sn the hybrid functional improves significantly upon semilocal functionals. α-Sn is predicted to be a metal using the PBE functional, causing an anomalous softening of the optical phonon modes at the Γ point, if the calculations are performed carefully using an accurate sampling of the Brillouin zone. We infer that an incorrect description of the electronic band structure can have a serious impact on other measurable materials properties, such as the phonon-dispersion relation, an effect that has been largely disregarded in literature. The HSE functional repairs the deficiency and predicts a semimetallic behavior for α-Sn allowing an accurate prediction of the vibrational properties of α-Sn.

Finally, for diamond we have carefully analyzed the overbending of the highest optical mode. We find that the hybrid functional reduces the overbending by about 1 meV compared to local and semilocal functionals, resulting in better overall agreement with experiment. We found overbending along all directions but Σ, where the dispersion is essentially flat. This is in agreement with experiments which are also hardly able to determine whether the optical mode overbends along Σ.

V. CONCLUSION

With the exception of α-Sn, semilocal and hybrid functionals yield very similar vibrational frequencies, with semilocal functionals tending to underestimate the vibrational frequencies and the hybrid HSE functional tending to overestimate the frequencies. The vibrational frequencies of the optical modes increase from LDA, over PBEsol toward PBE, and PBE generally gives best agreement with experiment at the experimental volume. Considering the huge computational effort of hybrid functionals, PBE seems to be the best pragmatic choice for phonon calculations, as long as the band structure is described qualitatively correct. For α-Sn this is not the case, and PBE predicts α-Sn to be a metal, resulting in a significant softening of the optical modes at Γ. In this case, only hybrid functionals yield qualitatively correct results.

ACKNOWLEDGMENTS

This work has been supported by the Austrian *Fonds zur Förderung der wissenschaftlichen Forschung* within the special research program *Infrared Optical Nanostructures (IR-ON)* and the START Project No. Y218.

*kerstin.hummer@univie.ac.at; http://cms.mpi.univie.ac.at/

[1] P. Hohenberg and W. Kohn, Phys. Rev. **136**, B864 (1964).
[2] W. Kohn and L. J. Sham, Phys. Rev. **140**, A1133 (1965).
[3] D. M. Ceperley, Phys. Rev. B **18**, 3126 (1978).
[4] D. M. Ceperley and B. J. Alder, Phys. Rev. Lett. **45**, 566 (1980).
[5] J. P. Perdew, K. Burke, and M. Ernzerhof, Phys. Rev. Lett. **77**, 3865 (1996).
[6] J. P. Perdew, K. Burke, and M. Ernzerhof, Phys. Rev. Lett. **78**, 1396 (1997).
[7] O. Gunnarsson and B. I. Lundqvist, Phys. Rev. B **13**, 4274 (1976).
[8] R. O. Jones and O. Gunnarsson, Rev. Mod. Phys. **61**, 689

(1989).
[9] W. Kohn, Rev. Mod. Phys. **71**, 1253 (1999).
[10] A. van de Walle and G. Ceder, Phys. Rev. B **59**, 14992 (1999).
[11] P. Pavone, K. Karch, O. Schütt, W. Windl, D. Strauch, P. Giannozzi, and S. Baroni, Phys. Rev. B **48**, 3156 (1993).
[12] P. Giannozzi, S. de Gironcoli, P. Pavone, and S. Baroni, Phys. Rev. B **43**, 7231 (1991).
[13] P. Pavone, S. Baroni, and S. de Gironcoli, Phys. Rev. B **57**, 10421 (1998).
[14] F. Favot and A. Dal Corso, Phys. Rev. B **60**, 11427 (1999).
[15] R. Armiento and A. E. Mattsson, Phys. Rev. B **72**, 085108 (2005).
[16] A. E. Mattsson, R. Armiento, J. Paier, G. Kresse, J. M. Wills, and T. R. Mattsson, J. Chem. Phys. **128**, 084714 (2008).
[17] J. P. Perdew, A. Ruzsinszky, G. I. Csonka, O. A. Vydrov, G. E. Scuseria, L. A. Constantin, X. Zhou, and K. Burke, Phys. Rev. Lett. **100**, 136406 (2008).
[18] A. E. Mattsson, R. Armiento, and T. R. Mattsson, Phys. Rev. Lett. **101**, 239701 (2008).
[19] B. G. Janesko, T. M. Henderson, and G. E. Scuseria, Phys. Chem. Chem. Phys. **11**, 443 (2009).
[20] J. Paier, M. Marsman, and G. Kresse, J. Chem. Phys. **127**, 024103 (2007).
[21] J. Heyd, G. E. Scuseria, and M. Ernzerhof, J. Chem. Phys. **118**, 8207 (2003).
[22] J. Heyd, G. E. Scuseria, and M. Ernzerhof, J. Chem. Phys. **124**, 219906 (2006).
[23] J. Heyd and G. E. Scuseria, J. Chem. Phys. **121**, 1187 (2004).
[24] To avoid confusion concerning the terminology, we would like to point out that HSE03 uses two different range-separation (*screening*) parameters μ for the HF part and for the DFT part, respectively, whereas the HSE06 employs a single parameter $\mu=0.11$ a.u.$^{-1}$ for both parts.
[25] A. V. Krukau, O. A. Vydrov, A. F. Izmaylov, and G. E. Scuseria, J. Chem. Phys. **125**, 224106 (2006).
[26] J. Paier, M. Marsman, K. Hummer, G. Kresse, I. C. Gerber, and J. G. Ángyán, J. Chem. Phys. **124**, 154709 (2006).
[27] J. Paier, M. Marsman, K. Hummer, G. Kresse, I. C. Gerber, and J. G. Ángyán, J. Chem. Phys. **125**, 249901 (2006).
[28] J. E. Peralta, J. Heyd, G. E. Scuseria, and R. L. Martin, Phys. Rev. B **74**, 073101 (2006).
[29] K. Hummer, A. Grüneis, and G. Kresse, Phys. Rev. B **75**, 195211 (2007).
[30] M. Marsman, J. Paier, A. Stroppa, and G. Kresse, J. Phys.: Condens. Matter **20**, 064201 (2008).
[31] A. Stroppa, K. Termentzidis, J. Paier, G. Kresse, and J. Hafner, Phys. Rev. B **76**, 195440 (2007).
[32] A. F. Izmaylov and G. E. Scuseria, J. Chem. Phys. **127**, 144106 (2007).
[33] A. F. Izmaylov and G. E. Scuseria, arXiv:0802.3385 (unpublished).
[34] R. Wahl, D. Vogtenhuber, and G. Kresse, Phys. Rev. B **78**, 104116 (2008).
[35] P. E. Blöchl, Phys. Rev. B **50**, 17953 (1994).
[36] G. Kresse and D. Joubert, Phys. Rev. B **59**, 1758 (1999).
[37] G. Kresse and J. Furthmüller, Comput. Mater. Sci. **6**, 15 (1996).
[38] G. Kresse and J. Furthmüller, Phys. Rev. B **54**, 11169 (1996).
[39] G. Kresse, J. Furthmüller, and J. Hafner, Europhys. Lett. **32**, 729 (1995).
[40] M. Born and K. Huang, *Dynamical Theory of Crystal Lattices* (Oxford University Press, Oxford, 1954).
[41] S. Baroni, S. de Gironcoli, A. Dal Corso, and P. Giannozzi, Rev. Mod. Phys. **73**, 515 (2001).
[42] N. W. Ashcroft and N. D. Mermin, *Solid State Physics* (Saunders College Publishing, Fort Worth, Texas, 1976).
[43] P. Pavone, J. Phys.: Condens. Matter **13**, 7593 (2001).
[44] In more detail, the force constants matrix in supercell calculations is given by $\tilde{C}_{i\alpha,j\beta}(\mathbf{R}_m-\mathbf{R}_n)=\Sigma_\tau C_{i\alpha,j\beta}(\mathbf{R}_m-\mathbf{R}_n+\tau)$, where τ are all lattice vectors of the supercell. It can be shown that for $\mathbf{q}$ commensurate with the supercell, $\tilde{C}_{i\alpha,j\beta}(\mathbf{q})$ is exact.
[45] *Landolt-Börnstein Semiconductors*, edited by O. Madelung, U. Rössler, and M. Schulz (Springer-Verlag, Berlin, Heidelberg, New York, 2002), Vol. 41.
[46] M. Y. Hu, H. Sinn, A. Alatas, W. Sturhahn, E. E. Alp, H.-C. Wille, Y. V. Shvydko, J. P. Sutter, J. Bandaru, E. E. Haller *et al.*, Phys. Rev. B **67**, 113306 (2003).
[47] D. L. Price and J. M. Rowe, Solid State Commun. **7**, 1433 (1969).
[48] Y. Ma and J. S. Tse, Solid State Commun. **143**, 161 (2007).
[49] F. F. Murnaghan, Proc. Natl. Acad. Sci. U.S.A. **30**, 244 (1944).
[50] H. J. Monkhorst and J. D. Pack, Phys. Rev. B **13**, 5188 (1976).
[51] F. Tran, R. Laskowski, P. Blaha, and K. Schwarz, Phys. Rev. B **75**, 115131 (2007).
[52] J. Heyd, J. Peralta, G. E. Scuseria, and R. L. Martin, J. Chem. Phys. **123**, 174101 (2005).
[53] P. Haas, F. Tran, and P. Blaha, Phys. Rev. B **79**, 085104 (2009); **79**, 209902(E) (2009).
[54] P. Y. Yu and M. Cardona, *Fundamentals of Semiconductors* (Springer-Verlag, Berlin, Heidelberg, New York, 2001).
[55] J. L. Warren, J. L. Yarnell, G. Dolling, and R. A. Cowley, Phys. Rev. **158**, 805 (1967).
[56] G. Dolling, *Inelastic Scattering of Neutrons in Solids and Liquids* (IAEA, Vienna, 1963), Vol. 2.
[57] G. Nilsson and G. Nelin, Phys. Rev. B **6**, 3777 (1972).
[58] G. Nilsson and G. Nelin, Phys. Rev. B **3**, 364 (1971).
[59] D. L. Price, J. M. Rowe, and R. M. Nicklow, Phys. Rev. B **3**, 1268 (1971).
[60] J. Kulda, H. Kainzmaier, D. Strauch, B. Dorner, M. Lorenzen, and M. Krisch, Phys. Rev. B **66**, 241202(R) (2002).
[61] M. Schwoerer-Böhning, A. T. Macrander, and D. A. Arms, Phys. Rev. Lett. **80**, 5572 (1998).
[62] E. Burkel, *Inelastic Scattering of X-Rays with Very High Energy Resolution* (Springer-Verlag, Berlin, Heidelberg, New York, 1991).
[63] J. Kulda, B. Dorner, B. Roessli, H. Sterner, R. Bauer, T. May, K. Karch, P. Pavone, and D. Strauch, Solid State Commun. **99**, 799 (1996).
[64] W. Windl, P. Pavone, K. Karch, O. Schütt, D. Strauch, P. Giannozzi, and S. Baroni, Phys. Rev. B **48**, 3164 (1993).
[65] D. Vanderbilt, S. G. Louie, and M. L. Cohen, Phys. Rev. Lett. **53**, 1477 (1984).
[66] S. Go, H. Bilz, and M. Cardona, Phys. Rev. Lett. **34**, 580 (1975).
[67] J. Kulda, D. Strauch, P. Pavone, and Y. Ishii, Phys. Rev. B **50**, 13347 (1994).